Title

Deterministic Assembly of Arrays of Lithographically Defined WS2 and MoS2 Monolayer Features Directly From Multilayer Sources Into Van Der Waals Heterostructures

Permalink

https://escholarship.org/uc/item/5c37588w

Journal

Journal of Micro and Nano-Manufacturing, 7(4)

ISSN

2166-0468

Authors

Nguyen, Vu
Gramling, Hannah
Towle, Clarissa
et al.

Publication Date

2019-12-01

DOI

10.1115/1.4045259

Supplemental Material

https://escholarship.org/uc/item/5c37588w#supplemental

Peer reviewed

Deterministic assembly of arrays of lithographically defined WS$_2$ and MoS$_2$ monolayer features directly from multilayer sources into van der Waals heterostructures

Vu Nguyen[□], Hannah Gramling[□], Clarissa Towle[§‡], Wan Li[※], Der-Hsien Lien[‖‡], Hyungjin Kim[‖‡], Daryl C. Chrzan[§‡], Ali Javey[‖‡], Ke Xu[※], Joel Ager[§‡], Hayden Taylor[□]*

[□]Department of Mechanical Engineering, [§]Department of Materials Science and Engineering, [‖]Department of Electrical Engineering and Computer Sciences, [※]Department of Chemistry, University of California, Berkeley, Berkeley, California 94720, United States

[‡]Materials Sciences Division, Lawrence Berkeley National Laboratories, Berkeley, California 94720, United States

*email contact: hkt@berkeley.edu

Abstract

One of the major challenges in the van der Waals (vdW) integration of 2D materials is achieving high-yield and high-throughput assembly of pre-defined sequences of monolayers into heterostructure arrays. Mechanical exfoliation has recently been studied as a promising technique to transfer monolayers from a multilayer source synthesized by other techniques, allowing the deposition of a wide variety of 2D materials without exposing the target substrate to harsh synthesis conditions. Although a variety of processes have been developed to exfoliate the 2D materials mechanically from the source and place them deterministically onto a target substrate, they can typically transfer only either a wafer-scale blanket or one small flake at a time with uncontrolled size and shape. Here we present a method to assemble arrays of lithographically defined monolayer WS_2 and MoS_2 features from multilayer sources and directly transfer them in a deterministic manner onto target substrates. This exfoliate–align–release process—without the need of an intermediate carrier substrate—is enabled by combining a patterned, gold-mediated exfoliation technique with a new optically transparent, heat-releasable adhesive. WS_2/MoS_2 vdW heterostructure arrays produced by this method show the expected interlayer exciton between the monolayers. Light-emitting devices using WS_2 monolayers were also demonstrated, proving the functionality of the fabricated materials. Our work demonstrates a significant step towards developing mechanical exfoliation as a scalable dry transfer technique for the manufacturing of functional, atomically thin materials.

1. Introduction

The ability to produce monolayers of transition metal dichalcogenides (TMDCs), which form a class of one-molecule-thick sheets with useful mechanical [1], electronic [2, 3] and optoelectronic [3-5] properties, has motivated intense research in their applications through van der Waals (vdW) integration with other 2D materials as well as with traditional semiconductor technologies [6, 7]. VdW integration [8, 9], the process of assembling dissimilar materials together using the universal vdW force, promises artificial

structures with controlled chemical composition, atomically sharp interfaces without the lattice matching requirement, and advanced material properties for applications such as tunneling transistors [10], light emitting devices [11, 12], photodetectors [13, 14] and silicon photonic integrated circuits [15]. The current state-of-the-art of vdW integration of 2D materials can produce either micro-scale heterostructures composed of as many as 29 layers [16], or continuous blanket heterostructures as large as 2-inch-wafer-scale [17, 18]. The techniques currently used for deterministically transferring micro-scale monolayer features, however, largely rely on features obtained from laborious and probabilistic 'Scotch-tape' exfoliation, and are limited to transferring individual features, which requires impractical repetitive placement to scale to large-area arrays [16, 19]. The most studied deterministic transfer technique for arrays of micro-features so far is micro-transfer printing, which uses an elastomeric polydimethylsiloxane (PDMS) stamp as the transfer medium with a controlled peeling rate to tune between pick-up (faster) and release (slower) modes [20, 21]. However, fully implementing such a technique requires a sophisticated and dedicated mechanical system and complex stamp design [22, 23]. Although PDMS stamps have been adopted in the transfer of 2D materials of many kinds [24-27], they still rely on an initial probabilistic exfoliation step, meaning that the size, shape and thickness of exfoliated layers are variable.

Recent advances in the chemical vapor deposition (CVD) of TMDC 2D crystals have provided large-area uniform sources, and the exfoliation-based transfer of wafer-scale continuous blankets of 2D materials could therefore be realized [17, 18]. However, large blanket transfer may easily trap contaminants, requires subsequent patterning steps which in turn potentially impose high etch-selectivity requirements on the fabrication of multiplexed heterostructures, and limits the complexity of the resultant heterostructures. Adoption of existing transfer techniques developed for pre-defined arrays of 3D materials—such as coating the arrays to be transferred with a carrier polymer layer—is a potential approach [28, 29], but in those cases a monolayer source is still required to yield monolayer exfoliation, which is key to achieving composition-controlled assembly of heterostructures. Although a recent exfoliation technique has achieved monolayer selectivity from multilayer CVD sources, it was only demonstrated for wafer-scale blanket layers [18].

In an effort to meet the need for a scalable technique to transfer pre-patterned monolayer arrays, we have recently developed a thin-film-mediated process to transfer arrays of TMDC monolayer features with pre-defined geometry directly from multilayer sources [30, 31]. A key advantage of this process is that it incorporates the use of an evaporated gold film which bonds to and strains the topmost monolayer of the TMDC source crystal, providing monolayer selectivity [32-34] and thus easing the layer-controlled requirement of the source. Therefore, millimeter-scale arrays of monolayer micro-features could be obtained in just one single exfoliation from multilayer source crystals of MoS_2 and WS_2 that are widely available in the general market. Nevertheless, although that process succeeded in pre-defining the *relative* positions of the micro-features being transferred, it did not control their *absolute* location on the target substrate. Moreover, the process used commercially available thermal release tape, which is opaque and is unsuitable for scaling down the transferred feature size because it contains heat-expandable microspheres. Thermal release tape also contains a proprietary adhesive polymer that is challenging to remove completely from the surfaces it touches [35]. Material residues were implicated in limiting the process's release yield and monolayer cleanliness, while the opacity of the tape inhibited accurate positioning on the substrate.

Here we present a deterministic assembly process compatible with existing semiconductor manufacturing equipment that can achieve fully position-controlled transfer of arrays of lithographically defined WS_2 and MoS_2 monolayer features from multilayer sources, thereby enabling straightforward stacking of optoelectronically functional vdW heterostructure arrays. We dub the new process Covalent-bond Exfoliate–Align–Release (CoBEARs). The process is enabled by the use of a transparent thermal release adhesive layer, which is fabricated from readily available materials using spin-coating to achieve uniform sample coverage. Positioning can be achieved with standard alignment equipment such as mask aligners and wafer bonders. The CoBEARs process is able to achieve monolayer selectivity in the exfoliation step thanks to the use of an evaporated Au film on the multilayer source. The maximum processing temperature required during monolayer deposition is only about 90 °C, which is needed to achieve the release of the micro-features onto the target substrate. Such a temperature is low enough to

enable integration with heat-susceptible substrates such as thermoplastic polymers. The release yield of the exfoliated micro-feature arrays from the adhesive to the target substrate is reliably close to 100%. The overall monolayer yield of the whole process is currently about 50%, which is mainly limited by the quality of the multilayer sources. Inspection of the obtained monolayers by optical microscopy, atomic force microscopy (AFM), photoluminescence (PL), and electroluminescence (EL) shows that they are clean and without polymeric residues, and provide functional material for light-emitting devices. The process was then repeated to produce WS_2/MoS_2 heterostructure arrays that show coupled excitonic emission. Our work therefore represents significant progress in the assembly of mechanically exfoliated 2D material arrays for manufacturing functional, atomically thin materials.

2. Materials and fabrication process

A schematic of the CoBEARs process is shown in Fig. 1. The WS_2 multilayer sources were obtained as crystals synthesized through chemical vapor transport (CVT) (HQ Graphene, Groningen, Netherlands), while the MoS_2 sources were naturally occurring crystals (Crystal Age, Bristol, UK). The as-received source crystals were prepared for exfoliation by applying patterned Au and photoresist handles using the procedure described in our previous work [30], which is summarized as follows. A 100 nm Au film was thermally evaporated on top of the TMDC crystal to provide monolayer exfoliation selectivity and also to protect the monolayer in subsequent processing steps. A 15 μ m-thick photoresist handle (AZ P4620, MicroChemicals GmbH) was then spun on and patterned. This photoresist served both to mask the subsequent etching steps that would define the size and shape of the micro-features (100 μ m × 100 μ m squares in this work), and then to offset the adhesive from the surface of the bulk crystal to prevent uncontrolled contact and exfoliation of thick TMDC layers. The etching consisted of two steps: a KI/I_2 wet etch to pattern the gold, followed by SF_6 plasma etching of the bulk 2D crystal (20 sccm, 200 W, 60 s, Plasma Equipment Technical Services, Inc.). The plasma etch was found to enhance the yield of exfoliation

and is thought to create crack initiation sites at the edges of the micro-features. Crucially, the plasma etch step does *not* need to be atomically precise, although we found that its duration could be optimized for monolayer exfoliation (details shown in Supplemental Fig. S1).

Immediately before the exfoliation step, the heat-releasable adhesive was fabricated by spin-coating a layer of low-crosslinked viscoelastic polymer (AZ P4620 photoresist, ~7 μ m thick, unbaked) onto a fluorinated ethylene propylene (FEP) film (127 μ m-thick film for Wanhao Duplicator, Amazon; Fig. 1, step 2). Details of the spin-coating parameters are provided in the supplemental material. FEP film was selected for its optical transparency, its high tendency to gain electrostatic charge [36] to enable temporary mounting onto a micromanipulator, and its low surface energy for effective release of the viscoelastic polymer layer. Despite the non-sticky nature of the FEP film, the viscoelastic polymer was successfully coated over its entire 25 mm × 25 mm area thanks to a high-acceleration spin recipe (1600 rpm/s ramp from rest to 2200 rpm, 2200 rpm for 1 minute, and then 1000 rpm for 20 s: supplemental Fig. S2). The FEP film spin-coated with the unbaked photoresist was used as an adhesive to exfoliate material from the bulk 2D crystal (Fig. 1, step 3). The exfoliation was typically done within three minutes of spin-coating, while the wet photoresist was still sufficiently tacky. It is worth reiterating that the Au layer and the patterned photoresist handle enabled an array of monolayer features to be obtained after one single exfoliation, instead of after repetitive exfoliations as are needed in the conventional Scotch-tape technique.

The adhesive, loaded with the exfoliated array of micro-features, was then mounted on a blank glass plate in a photomask aligner (OAI Series 200 Aligner) by electrostatic force. Glass and FEP lie at the two opposite ends of the empirical triboelectric series [36, 37], and thus tend to gain positive and negative charges, respectively, when brought into contact. Using this well-known effect, a bare FEP piece was gently rubbed against the glass plate to produce a certain amount of electrostatic charge, before the adhesive-coated FEP was placed on the rubbed location of the glass plate. Thanks to the transparency of the glass plate and the adhesive, the location of the array on the target substrate could be controlled using the microscope and manipulator setup of the mask aligner (Fig. 1, step 4). After the desired location had been

determined, the adhesive was firmly pressed against the target substrate using the manual Z-adjustment knob of the aligner, until the unbaked photoresist adhesive no longer visually deformed with further pressing, corresponding to the photoresist handle contacting the FEP backing (Fig. 1, step 5.1). The bonding between the adhesive and the target substrate was strong enough to defeat the weak electrostatic force when the glass plate was lifted, keeping the exfoliated array at the desired location and separating the FEP from the glass. The substrate could now be taken out of the mask aligner and placed on a hotplate at 90 °C for 90 s to melt the photoresist adhesive completely, which formed an encapsulation over the exfoliated array and clamped it to the target substrate. Alternatively, steps 5.1 and 5.2 in Fig. 1 could be combined into one step if the mask aligner has a heating capability. We were also able to perform this transfer procedure in a wafer bonder (AML AWB-08) in 5×10^{-6} Torr vacuum, where the 90 °C heating could be applied immediately after pressing, followed by lifting the glass plate (a dummy glass wafer). The ability to perform the transfer in a wafer bonder chamber, under vacuum, offers additional control of environmental conditions during the process. Nevertheless, all samples shown in this work were made in ambient cleanroom conditions.

After melting the adhesive, the FEP film could be easily peeled off the target substrate (Fig. 1, step 6), leaving the exfoliated array encapsulated with the melted viscoelastic polymer on the target substrate. Due to the low crosslinked nature of the now slightly baked photoresist, it could be visibly removed in acetone in 10 min (Fig. 1, step 7). An additional gentle O_2 plasma cleaning (15 W, 15 s, 300 mTorr, Plasma Equipment Technical Services, Inc.) was applied to clean all polymer residues completely from the substrate. Finally, the Au layer was etched away in KI/I_2 solution (Transene Gold Etchant Type TFA) for 2 min, followed by rinsing in DI water (step 8 in Fig. 1).

3.   Results and discussion

The array of micro-features was monitored by optical microscopy at each stage of the process (Fig. 2a), from exfoliation until after the last Au-etching step when the exposed monolayer was obtained. Using optical images, we can define three yield metrics that characterize the degree of success in the transfer of micro-features after important steps, as well as the final amount of monolayer area obtained. We term these metrics: *feature exfoliation yield*, *feature release yield*, and *monolayer yield*.

The *feature exfoliation yield* is defined as the ratio of the number of successfully exfoliated features on the adhesive (immediately after step 3 in Fig. 1) to the number of features brought into contact with the adhesive during that step. Sites where features had touched the adhesive but not successfully remained adhered to it, leading to failed exfoliation, could be readily recognized in optical images from indentations made by the photoresist handle into the wet photoresist adhesive (Fig. 2a). Successfully exfoliated material, in contrast, was visible as reflective gold squares on the adhesive. Both the numerator and the denominator of the feature exfoliation yield calculation were counted over the entire area of the adhesive piece used (low-magnification images of the whole exfoliated array on one sample are shown in Supplemental Fig. S3).

The *feature release yield* is defined as the ratio of the number of features successfully released from the adhesive onto the target substrate (immediately after step 7 in Fig. 1) to the number of successfully exfoliated features on the adhesive (immediately after step 3 in Fig. 1). The number of successfully exfoliated features is the same number that serves as the numerator in the calculation of feature exfoliation yield above.

The third yield metric, *the monolayer yield*, is defined as the ratio of the total monolayer area finally present on the target substrate to the total, ideal area of all features present on the target substrate. The monolayer regions were identified and confirmed using three independent methods: AFM (Fig. 2b), interpretation of the material's optical reflectance spectrum based on thin-film optical interference calculations [38, 39] and mapping (Fig. 2c and Supplemental Fig. S4), and determination of the material's characteristic PL peak (Supplemental Fig. S4).

A summary of the three yield metrics is shown in Fig. 2d, with the overall process yield of monolayer material being the product of all three numbers, and equaling, on average, 49% for WS_2 (N = 8 samples) and 51% for MoS_2 (N = 4 samples) (Supplemental Fig. S5). Although these yield values are certainly not yet comparable with the production standards of the semiconductor manufacturing industry, the process that we have demonstrated has the potential to accelerate the development of new types of optoelectronic devices based on exfoliated 2D materials. Importantly, the method deposits regions of material in *predictable* locations so that arrays of devices can be readily created on a target substrate. As we will see below, the deterministic placement also allows effective formation of 2D heterostructures.

The high feature release yield, typically 100%, was achieved mainly thanks to the non-sticky surface of the FEP film, which was easily and cleanly peeled off the lightly baked photoresist layer encapsulating the array on the substrate. Feature release yield was also promoted by the strong vdW adhesion of the monolayer to the clean SiO_2 surface, which was able to withstand the liquid acetone cleaning of the excess photoresist. It is important to note that although the micro-feature array was encapsulated in a layer of polymer during the release step, this polymer, the lightly baked AZ P4620 photoresist, is only slightly crosslinked thanks to the low-temperature process, and thus can be completely removed with acetone and gentle O_2 plasma. The smoothness of the AFM topography scan in Fig. 2b indicates that excess polymer was effectively cleaned. The ability to release micro-features reliably and cleanly with this encapsulation approach promises to address the weaknesses of the widely used commercial thermal release tape, which employs heat-expandable microspheres that limit the scaling down of transferred feature size [35], and leaves behind residue that requires an extended and high-power O_2 plasma-cleaning recipe [30].

The moderate monolayer yield—about 69% of the total feature area deposited on the target substrate—is apparently due to the inclusion of multilayer areas and the undesired removal of the monolayer areas. The inclusion of multilayer areas in the transferred material could be due to the gold film contacting multiple layers where the TMDC surface lacks atomic flatness, although further experimentation is needed to confirm this effect. The undesired removal of monolayer areas is found to be correlated to the O_2 plasma

9

cleaning in step 7 of Fig. 1. The effectiveness of the protection provided by the 100 nm-thick Au layer for the monolayer underneath in this cleaning step appeared to depend on how energetic the plasma cleaning recipe was, as shown in Fig. 3. For WS_2, a mild and short O_2 plasma recipe (with about 15 W power for 15 s) produced monolayer features with smoother surfaces, larger areas and more sharply defined edges than a more energetic and extended recipe (either 120 W power for 15 s or 15 W for 60 s). A similar effect was also observed for MoS_2, although in this case the sharpness of edge definition was less dependent on plasma parameters (Supplemental Fig. S6). Rough surfaces resembling nanoparticles scattered on the material have also been observed previously on monolayer features that had undergone energetic and extended O_2 plasma cleaning before the Au etch [30]. In that case, X-ray photoelectron spectroscopy suggested that some Au remained on the surface after cleaning [30]. As an alternative to the solution of using a mild and short O_2 plasma recipe, a thicker metal protection layer or a non-plasma-based recipe, such as atomic hydrogen cleaning [40], could be considered to remove polymer residue with minimal effect on the monolayer.

In this work we report the results of transfer onto SiO_2/Si substrates, although we have also tested our transfer process on other substrates such as Si, sapphire, and glass with comparable results. Using polymeric substrates, meanwhile, might conceivably affect yield or placement accuracy due to their higher thermal expansion coefficients, surface roughness, and greater mechanical compliance, although any such effects could likely be mitigated by lamination onto more rigid substrates.

While yield of the deposited arrays was studied by optical-microscopy-based characterization, their optoelectronic properties were revealed through photoluminescence (PL) spectra. The transferred TMDC monolayer arrays are inherently direct-bandgap semiconductors, so they exhibit a strong PL peak at a characteristic wavelength corresponding to the energy of the bandgap. The PL spectra of a randomly selected sample of monolayer spots in WS_2 and MoS_2 arrays are plotted in Fig. 4a and 4b, respectively. The average PL peak position in one representative WS_2 sample lies at 625 ± 13 nm (mean $\pm3\sigma$, N = 17). The slight variation of the peak position could be due to native defects in the monolayer, substrate defects, or

residual monolayer strain caused by the process. The presence of native defects seems the most likely explanation, considering the much more consistent PL peak position of the MoS_2 monolayer array (666 ± 3 nm: mean $\pm3\sigma$, N = 15), which went through the same process but was made from a different material source. The higher variation in PL peak position of the WS_2 samples than that of the MoS_2 samples was also recorded in our previous work [30], which used similar material sources. Potential optoelectronic application of the obtained monolayer material was demonstrated in a transient-mode two-terminal electroluminescence (EL) device [12], which is shown in Supplemental Fig. S7. We achieved tunable emission intensity of the EL device by varying both amplitude and frequency of the applied voltage, thus demonstrating the potential for light-emitting applications of monolayer material exfoliated using the process described in this work.

In addition to monolayer arrays, the CoBEARs process is also capable of producing heterostructure arrays by repeating the monolayer deposition steps (steps 1–8 in Fig. 1). In the example shown in this work (Fig. 5), a second monolayer array of WS_2 was overlaid onto a previously transferred MoS_2 monolayer array. Because the O_2 plasma cleaning in step 7 removes any exposed monolayer material from the substrate, the resulting heterostructure regions are confined to the Au area of the most recent deposition. The two arrays were purposefully offset in the horizontal direction so that about half of the area of each square feature is a heterostructure, and the other half is monolayer WS_2 for reference, as demonstrated in the high-magnification image in Fig. 5a. The transparency of the transfer medium allowed the deposition location of the WS_2 array to be controlled to within about ±5 μm of its intended position relative to the MoS_2, as determined by visual inspection of the alignment between the horizontal edges of the square features in Fig. 5a, and by the absence of any discernible relative rotation between the two material arrays. This level of alignment was achieved by simple visual feedback through the microscope objective of the mask aligner. It is expected that even tighter alignment tolerances could be achieved with the introduction of dedicated alignment marks to the exfoliation masks of the two materials.

The exposed parts of the first, MoS_2, monolayer array were etched away in the cleaning step (step 7) of the WS_2 deposition cycle, leaving 100 μm × 100 μm square areas of WS_2 monolayer and rectangular WS_2-on-MoS_2 heterostructures where the two arrays overlapped. Raman spectroscopy, shown in Fig. 5b, confirmed the presence of WS_2 monolayers and WS_2-on-MoS_2 heterostructures. WS_2/MoS_2 has been demonstrated to constitute a type II heterostructure that is promising for charge-separating devices such as photodetectors and photovoltaics [6, 13, 41]. Insights into the electrical properties of this type of heterostructure can be gained through simple PL measurements. The spatial separation of electron–hole pairs in this type of heterostructure—with holes (electrons) generated in the MoS_2 (WS_2) layer being swept to the WS_2 (MoS_2) layer—is evident from the quenching of the PL peaks of both individual monolayers due to inefficient recombination [41-43]. We studied this PL quenching effect in our fabricated WS_2-on-MoS_2 heterostructures before and after a short annealing (200 °C for 5 min in air), as shown in Fig. 5c. Before annealing, the heterostructures still exhibited two PL peaks, resembling the superposition of two independent monolayers, but with reduced intensities and a slight shift in peak positions compared to the individual monolayers. These pre-annealing spectra indicate that charge transfer had occurred and the electronic band structure of each monolayer had been influenced by the other layer. After annealing, the PL peaks corresponding to individual monolayers disappeared, and a single peak at a new longer wavelength than those of the monolayers emerged. The complete suppression of the PL peaks of individual monolayers suggests efficient photoexcited charge separation, and the new and relatively weak PL peak can be attributed to the less efficient recombination of spatially separated charges [43]. Since the charge transfer dominates only for short interlayer distances [42, 44], the annealing step could have driven the trapped species out of the heterojunction and brought the two layers into closer contact, thereby improving the charge separation.

4.   Conclusion

We have developed a manufacturing process, CoBEARs, to transfer arrays of molecularly thin TMDC micro-features directly and deterministically from multilayer sources to target substrates. CoBEARs augments an existing thin-film-mediated exfoliation technique with the use of an optically transparent thermal release adhesive that is compatible with standard semiconductor manufacturing equipment and processes, and specifically enables reliable multi-layer alignment. The CoBEARs process has been shown to achieve almost 100% feature release yield on a target SiO_2/Si substrate, and an overall areal monolayer yield of about 50%. Although the present overall areal yield is not yet comparable to semiconductor industry standards, the process can already greatly accelerate research into new devices made from 2D materials, because it offers a way of defining monolayer material in predictable locations, allowing for straightforward alignment with other functional materials or electrodes.

Characterization by optical microscopy, AFM, PL, and EL showed that the obtained monolayers were smooth and without polymeric residues, had spatially consistent optoelectronic properties, and could serve as a functional light-emitting device. The WS_2/MoS_2 heterostructure array obtained by the process exhibited the interlayer exciton with completely quenched intralayer excitons, which is expected of a type II heterostructure and potentially enables the design of next-generation photodetectors. CoBEARs therefore represents a significant step towards applying mechanical exfoliation as a transfer technique in the scalable manufacturing of multiplexed 2D material devices.

Sciences, Materials Sciences and Engineering Division of the U.S. Department of Energy, under Contract DE-AC02-05CH11231.

Nomenclature

Y_{exf} feature exfoliation yield

Y_{rel} feature release yield

Y_{mono} monolayer yield

σ sample standard deviation

Figure captions

Fig. 1: Schematic of the CoBEARs process. In this work, the prototypical adhesive used in step 2 is the same photoresist material (AZ P4620) used to pattern the features in step 1. The electrostatic charges in step 4 were produced by gently rubbing a bare FEP film against the glass, and then the adhesive film with exfoliated features was placed on the rubbed location. Step 5.2 could also be done before the glass is lifted in step 5.1 if the alignment tool also has heating capability. The green regions in step 8 represent monolayer exposed after the Au etch. The substrate after step 8 could be returned to step 4 repeatedly to produce arrays of heterostructures.

Fig. 2: Yield metrics of the process. (a) Optical microscopy images of the array of WS_2 micro-features after critical steps. The target substrate is 50 nm SiO_2/Si. The monolayer array is obtained after one single exfoliation. Scale bars are 200 μm. (b) AFM topography scan at the edge of a monolayer feature in (a), showing a smooth surface with a step height consistent with monolayer. Scale bar is 1 μm. (c) false color mapping of the monolayer region in (a), which is determined by comparing the contrast under 532 nm

illumination (Supplemental Fig. S3) with the theoretical contrast calculated with a thin film interference model [38, 39]. The areas where measured contrast agree with calculated monolayer contrast are marked as red, and black otherwise. Scale bars are 200 μm. (d) summary of the yields calculated after the three steps in (a): feature exfoliation yield Y_{exf}, feature release yield Y_{rel}, and monolayer yield, Y_{mono}. Error bars are ±1 sample standard deviation with N = 8 samples.

Fig. 3: Effect of O_2 plasma cleaning on the surface roughness and edge definition of WS_2 features. (a–d): Optical microscope images of monolayers obtained following various cleaning recipes performed in step 7 of Fig. 1. All scale bars are 100 μm. Images shown are after etching of the gold, as in step 8 of Fig. 1. (e–f): AFM topography scans of features in (a–d), respectively. 'Sq' denotes the root-mean-square surface roughness of the scanned area. All AFM scans shown are of a 5 μm-square region.

Fig. 4: Optoelectronic characterization. Photoluminescence spectra of a randomly selected sample of spots in (a) the WS_2 sample and (b) the MoS_2 sample obtained through CoBEARs. All scale bars are 200 μm. PL peak wavelengths were 625±13 nm for WS_2 and 666±3 nm for MoS_2 (±3 sample standard deviations in each case).

Fig. 5: Assembly and characterization of a heterostructure array. (a) WS_2/MoS_2 heterostructure array obtained by performing the steps in Fig. 1, with the first cycle depositing MoS_2 and the second cycle depositing WS_2. From left to right, scale bars are 200 μm, 200 μm and 100 μm. (b) Raman spectra of the samples in (a). The MoS_2-only spectrum was obtained before WS_2 deposition. The WS_2-only and WS_2/MoS_2 spectra, obtained after annealing, correspond to the two red spots numbered 1 and 2 respectively in the high-magnification image of (a). (c) PL spectra showing the coupled exciton exhibited

by the WS$_2$/MoS$_2$ heterostructure that emerges after annealing at 200 °C for 5 min. The four replicate PL spectra, 1–4 in both the before- and after-annealing states, correspond to the locations shown by numbered green dots in (a).

References

1.   Bertolazzi, S., Brivio, J. and Kis, A., 2011. Stretching and breaking of ultrathin MoS2. *ACS Nano*, *5*(12), pp.9703-9709.

2.   Radisavljevic, B., Radenovic, A., Brivio, J., Giacometti, V. and Kis, A., 2011. Single-layer MoS 2 transistors. *Nature Nanotechnology*, *6*(3), p.147.

3.   Mak, K.F., Lee, C., Hone, J., Shan, J. and Heinz, T.F., 2010. Atomically thin MoS 2: a new direct-gap semiconductor. *Physical Review Letters*, *105*(13), p.136805.

4.   Splendiani, A., Sun, L., Zhang, Y., Li, T., Kim, J., Chim, C.Y., Galli, G. and Wang, F., 2010. Emerging photoluminescence in monolayer MoS2. *Nano Letters*, *10*(4), pp.1271-1275.

5.   Gutiérrez, H.R., Perea-López, N., Elías, A.L., Berkdemir, A., Wang, B., Lv, R., López-Urías, F., Crespi, V.H., Terrones, H. and Terrones, M., 2012. Extraordinary room-temperature photoluminescence in triangular WS2 monolayers. *Nano Letters*, *13*(8), pp.3447-3454.

6.   Shim, J., Kang, D.H., Kim, Y., Kum, H., Kong, W., Bae, S.H., Almansouri, I., Lee, K., Park, J.H. and Kim, J., 2018. Recent progress in Van der Waals (vdW) heterojunction-based electronic and optoelectronic devices. *Carbon*, *133*, pp.78-89.

7.   Wachter, S., Polyushkin, D.K., Bethge, O. and Mueller, T., 2017. A microprocessor based on a two-dimensional semiconductor. *Nature Communications*, *8*, p.14948.

8.   Geim, A.K. and Grigorieva, I.V., 2013. Van der Waals heterostructures. *Nature*, *499*(7459), p.419.

9.   Liu, Y., Huang, Y. and Duan, X., 2019. Van der Waals integration before and beyond two-dimensional materials. *Nature*, *567*(7748), p.323.

10.   Roy, T., Tosun, M., Cao, X., Fang, H., Lien, D.H., Zhao, P., Chen, Y.Z., Chueh, Y.L., Guo, J. and Javey, A., 2015. Dual-gated MoS2/WSe2 van der Waals tunnel diodes and transistors. *ACS Nano*, *9*(2), pp.2071-2079.

11.   Withers, F., Del Pozo-Zamudio, O., Mishchenko, A., Rooney, A.P., Gholinia, A., Watanabe, K., Taniguchi, T., Haigh, S.J., Geim, A.K., Tartakovskii, A.I. and Novoselov, K.S., 2015. Light-emitting diodes by band-structure engineering in van der Waals heterostructures. *Nature Materials*, *14*(3), p.301.

12.   Lien, D.H., Amani, M., Desai, S.B., Ahn, G.H., Han, K., He, J.H., Ager, J.W., Wu, M.C. and Javey, A., 2018. Large-area and bright pulsed electroluminescence in monolayer semiconductors. *Nature communications*, *9*(1), p.1229.

13.   Wang, G., Li, L., Fan, W., Wang, R., Zhou, S., Lü, J.T., Gan, L. and Zhai, T., 2018. Interlayer coupling induced infrared response in WS2/MoS2 heterostructures enhanced by surface plasmon resonance. *Advanced Functional Materials*, *28*(22), p.1800339.

14.   Zhang, K., Zhang, T., Cheng, G., Li, T., Wang, S., Wei, W., Zhou, X., Yu, W., Sun, Y., Wang, P. and Zhang, D., 2016. Interlayer transition and infrared photodetection in atomically thin type-II MoTe2/MoS2 van der Waals heterostructures. *ACS Nano*, *10*(3), pp.3852-3858.

15.   Bie, Y.Q., Grosso, G., Heuck, M., Furchi, M.M., Cao, Y., Zheng, J., Bunandar, D., Navarro-Moratalla, E., Zhou, L., Efetov, D.K. and Taniguchi, T., 2017. A MoTe 2-based light-emitting diode and photodetector for silicon photonic integrated circuits. *Nature Nanotechnology*, *12*(12), p.1124.

16.   Masubuchi, S., Morimoto, M., Morikawa, S., Onodera, M., Asakawa, Y., Watanabe, K., Taniguchi, T. and Machida, T., 2018. Autonomous robotic searching and assembly of two-dimensional crystals to build van der Waals superlattices. *Nature Communications*, *9*(1), p.1413.

17.   Kang, K., Lee, K.H., Han, Y., Gao, H., Xie, S., Muller, D.A. and Park, J., 2017. Layer-by-layer assembly of two-dimensional materials into wafer-scale heterostructures. *Nature*, *550*(7675), p.229.

18.   Shim, J., Bae, S.H., Kong, W., Lee, D., Qiao, K., Nezich, D., Park, Y.J., Zhao, R., Sundaram, S., Li, X. and Yeon, H., 2018. Controlled crack propagation for atomic precision handling of wafer-scale two-dimensional materials. *Science*, *362*(6415), pp.665-670.

19.   Frisenda, R., Navarro-Moratalla, E., Gant, P., De Lara, D.P., Jarillo-Herrero, P., Gorbachev, R.V. and Castellanos-Gomez, A., 2018. Recent progress in the assembly of nanodevices and van der Waals heterostructures by deterministic placement of 2D materials. *Chemical Society Reviews*, *47*(1), pp.53-68.

20.   Meitl, M.A., Zhu, Z.T., Kumar, V., Lee, K.J., Feng, X., Huang, Y.Y., Adesida, I., Nuzzo, R.G. and Rogers, J.A., 2006. Transfer printing by kinetic control of adhesion to an elastomeric stamp. *Nature Materials*, *5*(1), p.33.

21.   Kim, C., Yoon, M.A., Jang, B., Kim, J.H., Lee, H.J. and Kim, K.S., 2017. Ultimate Control of Rate-Dependent Adhesion for Reversible Transfer Process via a Thin Elastomeric Layer. *ACS Applied Materials & Interfaces*, *9*(14), pp.12886-12892.

22.   Saeidpourazar, R., Sangid, M.D., Rogers, J.A. and Ferreira, P.M., 2012. A prototype printer for laser driven micro-transfer printing. *Journal of Manufacturing Processes*, *14*(4), pp.416-424.

23.   Kim, S., Wu, J., Carlson, A., Jin, S.H., Kovalsky, A., Glass, P., Liu, Z., Ahmed, N., Elgan, S.L., Chen, W. and Ferreira, P.M., 2010. Microstructured elastomeric surfaces with reversible adhesion and examples of their use in deterministic assembly by transfer printing. *Proceedings of the National Academy of Sciences*, *107*(40), pp.17095-17100.

24.   Ma, X., Liu, Q., Xu, D., Zhu, Y., Kim, S., Cui, Y., Zhong, L. and Liu, M., 2017. Capillary-force-assisted clean-stamp transfer of two-dimensional materials. *Nano Letters*, *17*(11), pp.6961-6967.

25.   Kim, K., Yankowitz, M., Fallahazad, B., Kang, S., Movva, H.C., Huang, S., Larentis, S., Corbet, C.M., Taniguchi, T., Watanabe, K. and Banerjee, S.K., 2016. van der Waals heterostructures with high accuracy rotational alignment. *Nano Letters*, *16*(3), pp.1989-1995.

26.   Pizzocchero, F., Gammelgaard, L., Jessen, B.S., Caridad, J.M., Wang, L., Hone, J., Bøggild, P. and Booth, T.J., 2016. The hot pick-up technique for batch assembly of van der Waals heterostructures. *Nature Communications*, *7*, p.11894.

27. Castellanos-Gomez, A., Buscema, M., Molenaar, R., Singh, V., Janssen, L., Van Der Zant, H.S. and Steele, G.A., 2014. Deterministic transfer of two-dimensional materials by all-dry viscoelastic stamping. *2D Materials*, *1*(1), p.011002.

28. Cheng, R., Bai, J., Liao, L., Zhou, H., Chen, Y., Liu, L., Lin, Y.C., Jiang, S., Huang, Y. and Duan, X., 2012. High-frequency self-aligned graphene transistors with transferred gate stacks. *Proceedings of the National Academy of Sciences*, *109*(29), pp.11588-11592.

29. Yan, Z., Han, M., Shi, Y., Badea, A., Yang, Y., Kulkarni, A., Hanson, E., Kandel, M.E., Wen, X., Zhang, F. and Luo, Y., 2017. Three-dimensional mesostructures as high-temperature growth templates, electronic cellular scaffolds, and self-propelled microrobots. *Proceedings of the National Academy of Sciences*, *114*(45), pp.E9455-E9464.

30. Gramling, H.M., Towle, C.M., Desai, S.B., Sun, H., Lewis, E.C., Nguyen, V.D., Ager, J.W., Chrzan, D., Yeatman, E.M., Javey, A. and Taylor, H., 2019. Spatially Precise Transfer of Patterned Monolayer WS$_2$ and MoS$_2$ with Features Larger than 10^4 μm^2 Directly from Multilayer Sources. *ACS Applied Electronic Materials*, *1*(3), pp.407-416.

31. Desai, S.B., Madhvapathy, S.R., Amani, M., Kiriya, D., Hettick, M., Tosun, M., Zhou, Y., Dubey, M., Ager III, J.W., Chrzan, D. and Javey, A., 2016. Gold-mediated exfoliation of ultralarge optoelectronically-perfect monolayers. *Advanced Materials*, *28*(21), pp.4053-4058.

32. Sun, H., Sirott, E.W., Mastandrea, J., Gramling, H.M., Zhou, Y., Poschmann, M., Taylor, H.K., Ager, J.W. and Chrzan, D.C., 2018. Theory of thin-film-mediated exfoliation of van der Waals bonded layered materials. *Physical Review Materials*, *2*(9), p.094004.

33. Velický, M., Donnelly, G.E., Hendren, W.R., McFarland, S., Scullion, D., DeBenedetti, W.J., Correa, G.C., Han, Y., Wain, A.J., Hines, M.A. and Muller, D.A., 2018. Mechanism of gold-assisted exfoliation of centimeter-sized transition-metal dichalcogenide monolayers. *ACS Nano*, *12*(10), pp.10463-10472.

34. Magda, G.Z., Pető, J., Dobrik, G., Hwang, C., Biró, L.P. and Tapasztó, L., 2015. Exfoliation of large-area transition metal chalcogenide single layers. *Scientific Reports*, *5*, p.14714.

35. Doi, T., Shimokawa, D. and Arimitsu, Y., Nitto Denko Corp, 2010. *Method of thermal adherend release and apparatus for thermal adherend release*. U.S. Patent 7,641,760.

36. Zi, Y., Niu, S., Wang, J., Wen, Z., Tang, W. and Wang, Z.L., 2015. Standards and figure-of-merits for quantifying the performance of triboelectric nanogenerators. *Nature Communications*, *6*, p.8376.

37. McCarty, L.S. and Whitesides, G.M., 2008. Electrostatic charging due to separation of ions at interfaces: contact electrification of ionic electrets. *Angewandte Chemie International Edition*, *47*(12), pp.2188-2207.

38. Benameur, M.M., Radisavljevic, B., Héron, J.S., Sahoo, S., Berger, H. and Kis, A., 2011. Visibility of dichalcogenide nanolayers. *Nanotechnology*, *22*(12), p.125706.

39. Li, Y., Chernikov, A., Zhang, X., Rigosi, A., Hill, H.M., van der Zande, A.M., Chenet, D.A., Shih, E.M., Hone, J. and Heinz, T.F., 2014. Measurement of the optical dielectric function of monolayer transition-metal dichalcogenides: MoS_2, $MoSe_2$, WS_2, and WSe_2. *Physical Review B*, *90*(20), p.205422.

40. Bell, G.R., Kaijaks, N.S., Dixon, R.J. and McConville, C.F., 1998. Atomic hydrogen cleaning of polar III–V semiconductor surfaces. *Surface Science*, *401*(2), pp.125-137.

41. Hong, X., Kim, J., Shi, S.F., Zhang, Y., Jin, C., Sun, Y., Tongay, S., Wu, J., Zhang, Y. and Wang, F., 2014. Ultrafast charge transfer in atomically thin MoS_2/WS_2 heterostructures. *Nature Nanotechnology*, *9*(9), p.682.

42. Tongay, S., Fan, W., Kang, J., Park, J., Koldemir, U., Suh, J., Narang, D.S., Liu, K., Ji, J., Li, J. and Sinclair, R., 2014. Tuning interlayer coupling in large-area heterostructures with CVD-grown MoS_2 and WS_2 monolayers. *Nano Letters*, *14*(6), pp.3185-3190.

43. Zhang, J., Wang, J., Chen, P., Sun, Y., Wu, S., Jia, Z., Lu, X., Yu, H., Chen, W., Zhu, J. and Xie, G., 2016. Observation of strong interlayer coupling in MoS_2/WS_2 heterostructures. *Advanced Materials*, *28*(10), pp.1950-1956.

44.   Xu, W., Kozawa, D., Liu, Y., Sheng, Y., Wei, K., Koman, V.B., Wang, S., Wang, X., Jiang, T., Strano, M.S. and Warner, J.H., 2018. Determining the optimized interlayer separation distance in vertical stacked 2D WS2: hBN: MoS2 heterostructures for exciton energy transfer. *Small*, *14*(13), p.1703727.

1. Pattern Au on flake

Photoresist
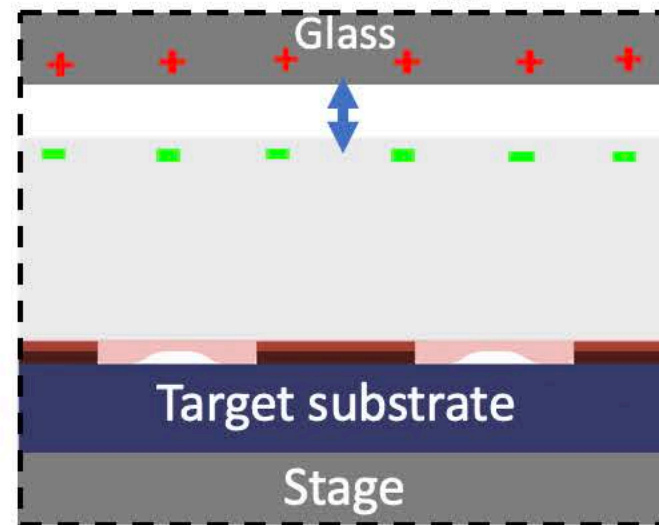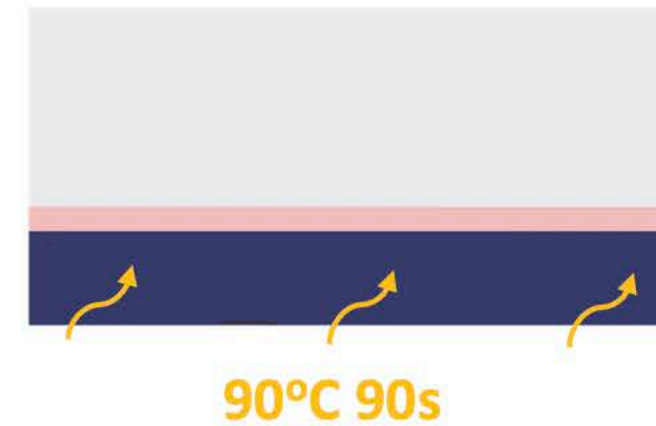Au
TMDC flake
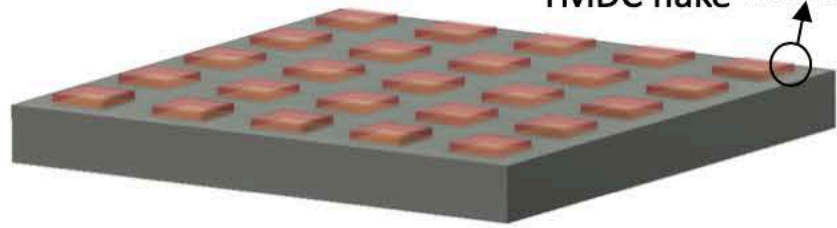
2. Spin-coat adhesive on FEP film

FEP

3. Exfoliate

FEP
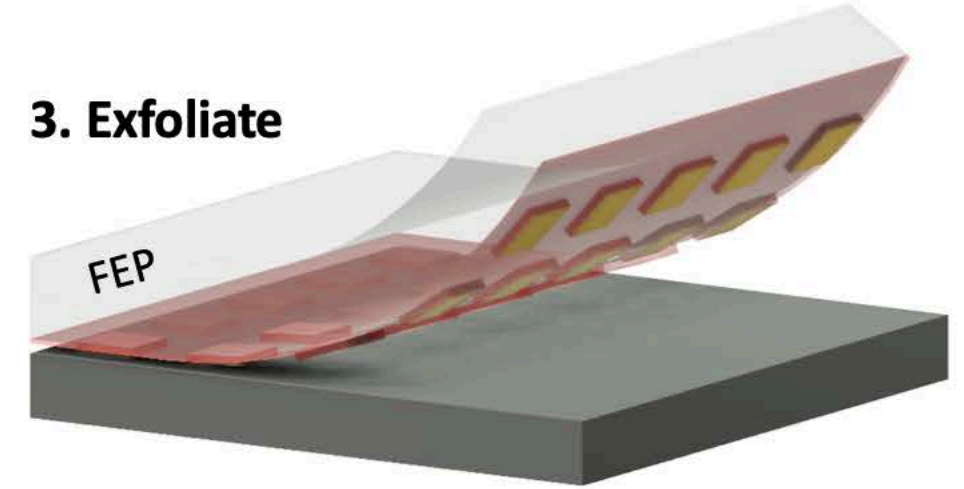
4. Align to desired location

Lens

Glass

+ + + + + +

− − − − − −

FEP

Target substrate

Stage

5.1. Press and lift glass

Glass

+ + + + + +

− − − − − −

Target substrate

Stage
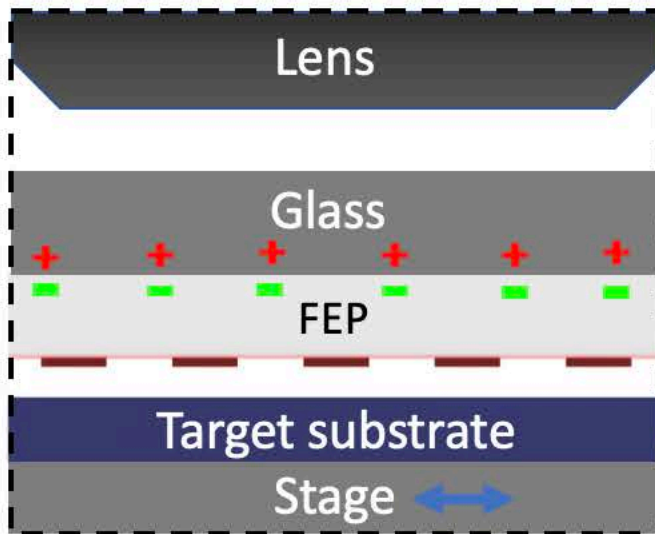
5.2. Melt adhesive/photoresist

90°C 90s

6. Release features by peeling off FEP film
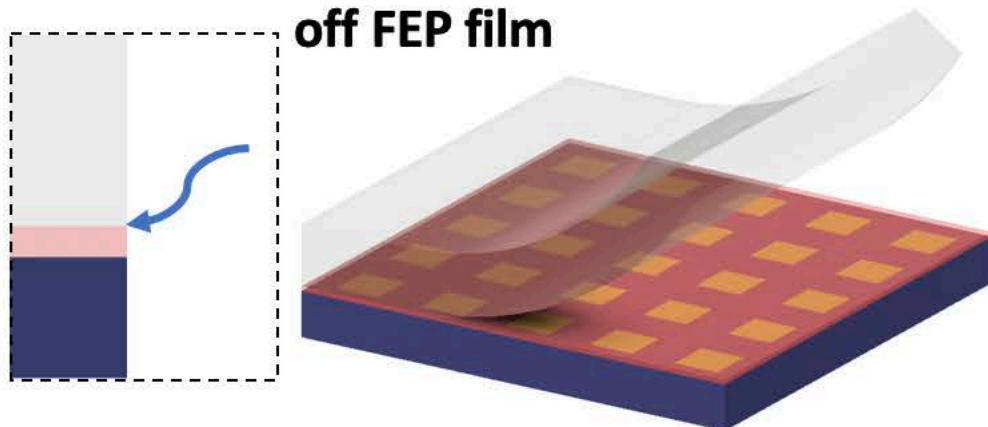
7. Remove adhesive/photoresist by acetone and O_2 plasma
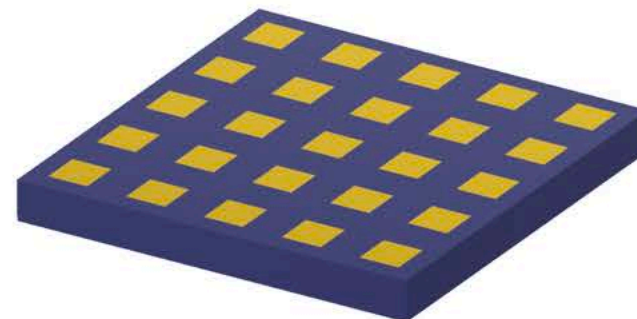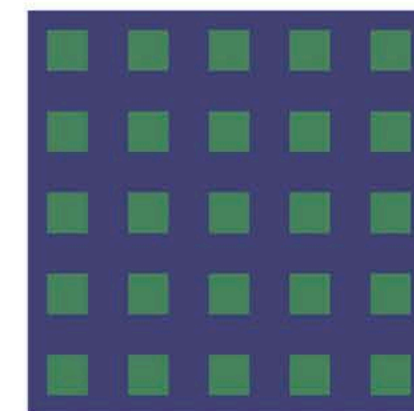
8. Etch Au

9. Repeat step 1-8 to produce heterostructure

a) No contact · Contact sites but no feature

b) 0.8nm

c)

d) Process yield

Y_{exf} Y_{rel} Y_{mono}

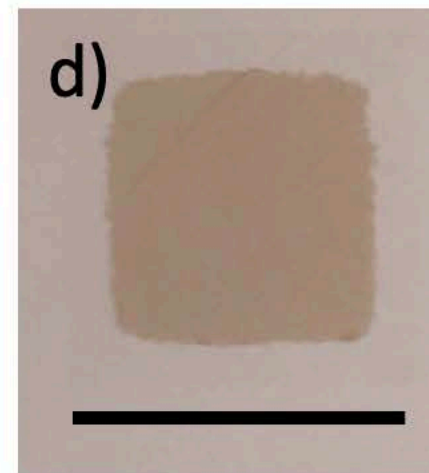**7. Remove adhesive/photoresist by acetone and O_2 plasma**

8. Etch Au
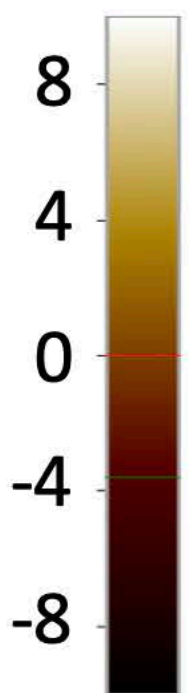
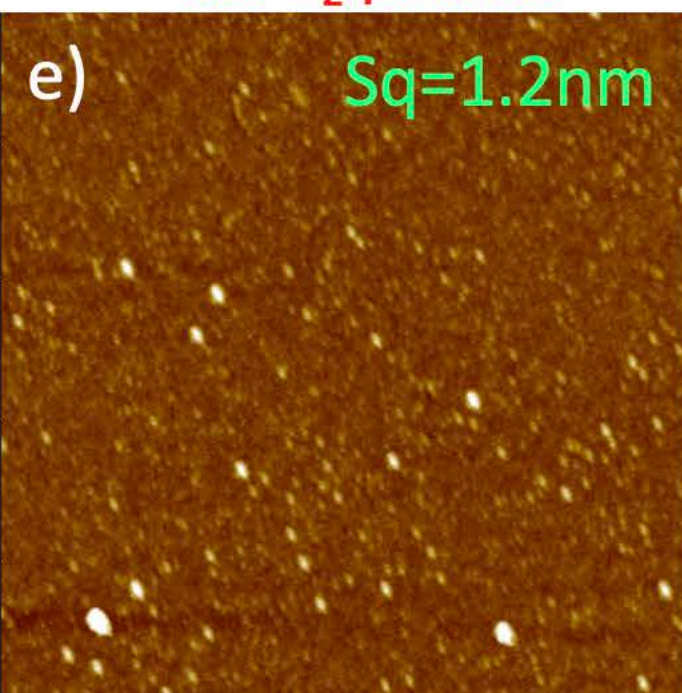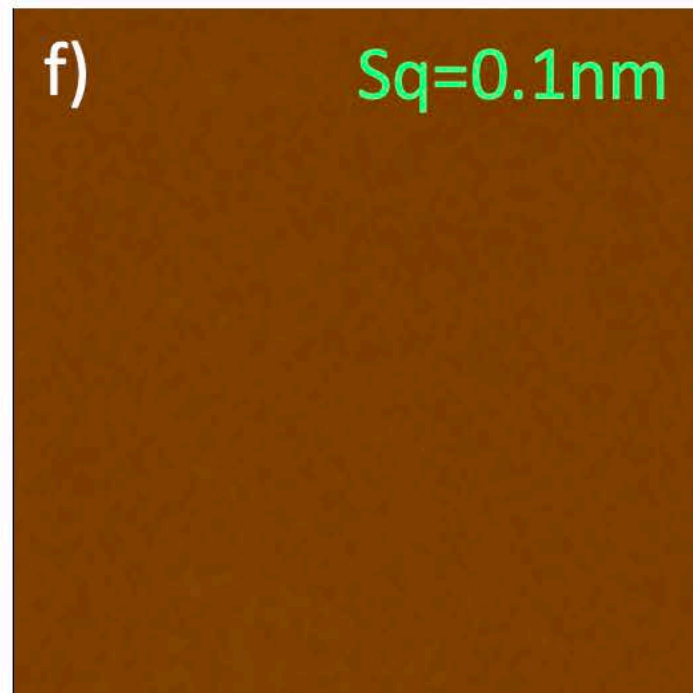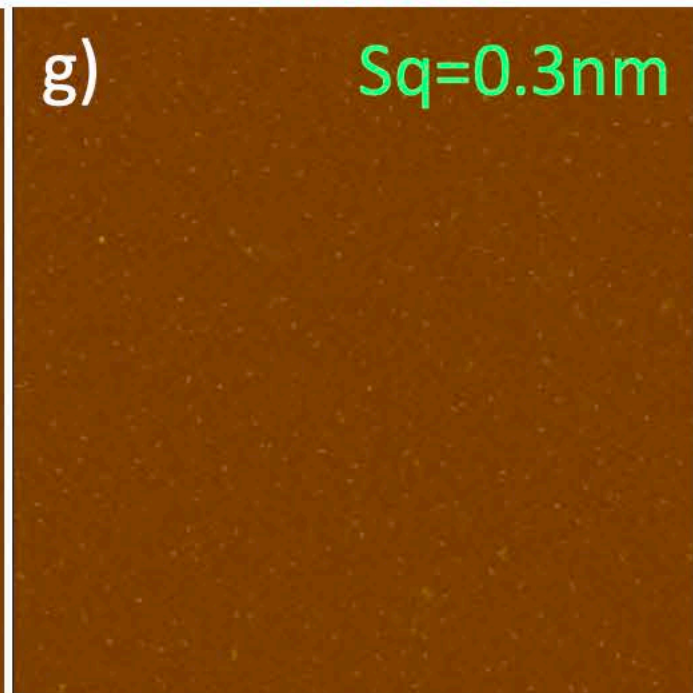2D material

a) b) c) d)

No O_2 plasma   15W 15s   15W 60s   120W 15s

No O_2 plasma   15W 15s   15W 60s   120W 15s

nm

8

4

0

-4

-8

e) Sq=1.2nm   f) Sq=0.1nm   g) Sq=0.3nm   h) Sq=1.1nm

5μmx5μm

a) WS₂

b) MoS₂

a)

MoS$_2$ WS$_2$ on MoS$_2$

1   4
1   2
2   3

b)

MoS$_2$ only

WS$_2$ only

WS$_2$/MoS$_2$

Raman intensity (a.u.)

Raman shift (cm^{-1})

c)

PL (counts s^{-1})

Wavelength (nm)

- - before annealing 1
—— after annealing 1
- - before annealing 2
—— after annealing 2
- - before annealing 3
—— after annealing 3
- - before annealing 4
—— after annealing 4